The Astrophysical Journal, 601:228–241, 2004 January 20

THE OFPE/WN9 STARS IN M33[1]

Luciana Bianchi
Center for Astrophysical Sciences, Johns Hopkins University, 239 Bloomberg Center for Physics and Astronomy, 3400 North Charles Street, Baltimore, MD 21218; bianchi@pha.jhu.edu

Ralph Bohlin
Space Telescope Science Institute, 3700 San Martin Drive, Baltimore, MD 21218

and

Philip Massey
Lowell Observatory, 1400 West Mars Hill Road, Flagstaff, AZ 86001
Received 2003 August 7; accepted 2003 November 3

ABSTRACT

We present *Hubble Space Telescope*/STIS Ultraviolet spectra of the six known Ofpe/WN9 stars ("slash stars") in M33. These stars were selected for showing the characteristics of the Ofpe/WN9 class from previous optical ground-based spectroscopy. The UV spectra are rich in wind lines whose strength and terminal velocity vary greatly across our target sample. We analyze the STIS spectra with non-LTE, line-blanketed, spherical models with hydrodynamics, computed with the WM-BASIC code. We find C to be underabundant and N overabundant with respect to the solar values, with a ratio (by mass) of C/N between 0.02 and 0.9 across the sample. Some stars show very conspicuous wind lines (P Cygni profiles), while two stars have extremely weak winds. The mass-loss rates thus vary greatly across the sample. The mass-loss rates of the hottest stars are lower than typical values of WNL stars but higher than expected for normal Population I massive stars. There is indication that the mass-loss rates may be variable in time. The C/N ratio and the other physical parameters derived by the spectral modeling ($T_{\rm eff}$, $L_{\rm bol}$, mass) are consistent with evolutionary calculations for objects with moderately high initial masses ($\approx$30–50 $M_{\odot}$), evolving toward the WNL stage through an enhanced mass-loss phase.

Subject headings: stars: abundances — stars: early-type — stars: evolution — stars: fundamental parameters — stars: mass loss — galaxies: individual (M33)

On-line material: color figures

1. INTRODUCTION

There is a general consensus about the Wolf-Rayet (W-R) stars being formed from O stars through high mass loss phases, but many specific questions remain unanswered. The Ofpe/WN9 star ("slash star") class, introduced by Walborn (1977, 1982a), shows properties intermediate between those of Of and WN stars: the emission is stronger than in the most extreme Of stars, but He II photospheric absorption indicates a less dense wind than seen in any W-R stars (see Bohannan & Walborn 1989). The implication is that Ofpe/WN9 stars are transitional objects between the Of and W-R stars in the "Conti scenario" (Conti 1976; Conti & Bohannan 1989). On the basis of the reduced surface H fraction observed in these stars, Pasquali et al. (1997) suggest instead the sequence O $\rightarrow$ Of $\rightarrow$ H-rich WNL $\rightarrow$ Ofpe/WN9 for initial masses of less than 100 $M_{\odot}$. One of the prototypes of the Ofpe/WN9 stars, R127 (HDE 269858) underwent an S Dor–like eruption in 1982 (Walborn 1982b; Stahl et al. 1983) revealing luminous blue variable (LBV) characteristics. Other evidence suggests that at least some of the Ofpe/WN9 stars have progenitors that are considerably lower in mass than the WNL stars; see Massey, DeGioia-Eastwood, & Waterhouse (2001). LBV irregular episodes of extreme mass loss may play an important role in the formation of W-R stars by substantial shedding of the progenitor's outer layers (e.g., Maeder & Conti 1994).

Ten "slash stars" are known in the LMC (Bohannan & Walborn 1989). Seven LMC Ofpe/WN9 stars were investigated in the optical (Nota et al. 1996) and in the UV with Faint Object Spectrograph (FOS) spectra (Pasquali et al. 1997) and with IR spectroscopy (Morris et al (1996). The spectral morphology confirms the transitional nature of these objects and their resemblance to LBVs. Crowther & Smith 1997 also analyzed optical spectra of LMC Ofpe/WN9 stars and reclassified them as WNL stars. Krabbe et al. (1991) observed a number of He I emission-line stars in the Galactic center whose He I line ratios and line-to-continuum ratios are consistent with Ofpe/WN9 stars. An Ofpe/WN9 star in NGC 300 was reported by Bresolin et al. (2002).

With follow-up ground-based (KPNO and MMT) spectroscopy of about 400 UV-brightest stellar sources found in the Ultraviolet Imaging Telescope (UIT) far- and near-UV (FUV and NUV) images of M33, we discovered six Ofpe/WN9 stars in this galaxy (Massey et al. 1996, hereafter MBHS). The "slash stars" are UV bright. In our study of the UIT UV-brightest sources in M33, these stars are relatively well separated from other stars in the $U-B$ versus FUV$-$NUV color-color diagram. They lie near the LBV candidates. Their colors are consistent with the fact that the Balmer jump is in *emission* in Ofpe/WN9 stars, which requires both high UV flux and an extended atmosphere, consistent with the strong P Cygni profiles (e.g., He I λ4471) characteristic of the Ofpe/WN9 class.

We present Space Telescope Imaging Spectrograph (STIS) ultraviolet spectra of the six known Ofpe/WN9 stars in M33. In § 2 details are given about the observations and the

[1] Based on observations with the *Hubble Space Telescope* which is operated by AURA, Inc., under NASA contract NAS5-26555.

reduction, and in § 3 the STIS UV spectra are analyzed with non-LTE, line-blanketed, hydrodynamical, spherical model atmospheres to derive physical stellar parameters. The results are interpreted in terms of stellar evolution by comparison with evolutionary model predictions (§ 4).

2. THE PROGRAMS STARS: DATA AND REDUCTION

2.1. *The Program Stars*

In Bianchi's *Hubble Space Telescope* (*HST*) program GO8207, we obtained UV spectra of the six Ofpe/WN9 stars known in M33. The spectra are shown in Figure 1. The objects were classified as Ofpe/WN9 from ground-based (KPNO and MMT) classification spectra of the UV-brightest stellar sources measured in the UIT far-UV and near-UV images (MBHS). The optical spectra, taken several years earlier (1993–1995), are shown in Figure 2 for the purpose of discussion in the following sections. A seventh object (M33-UIT339) was included in our program because of its photometric properties (Hα emission-line source). An additional object, M33-UIT340, was included serendipitously in the STIS long slit during the M33-UIT339 observations by choosing an

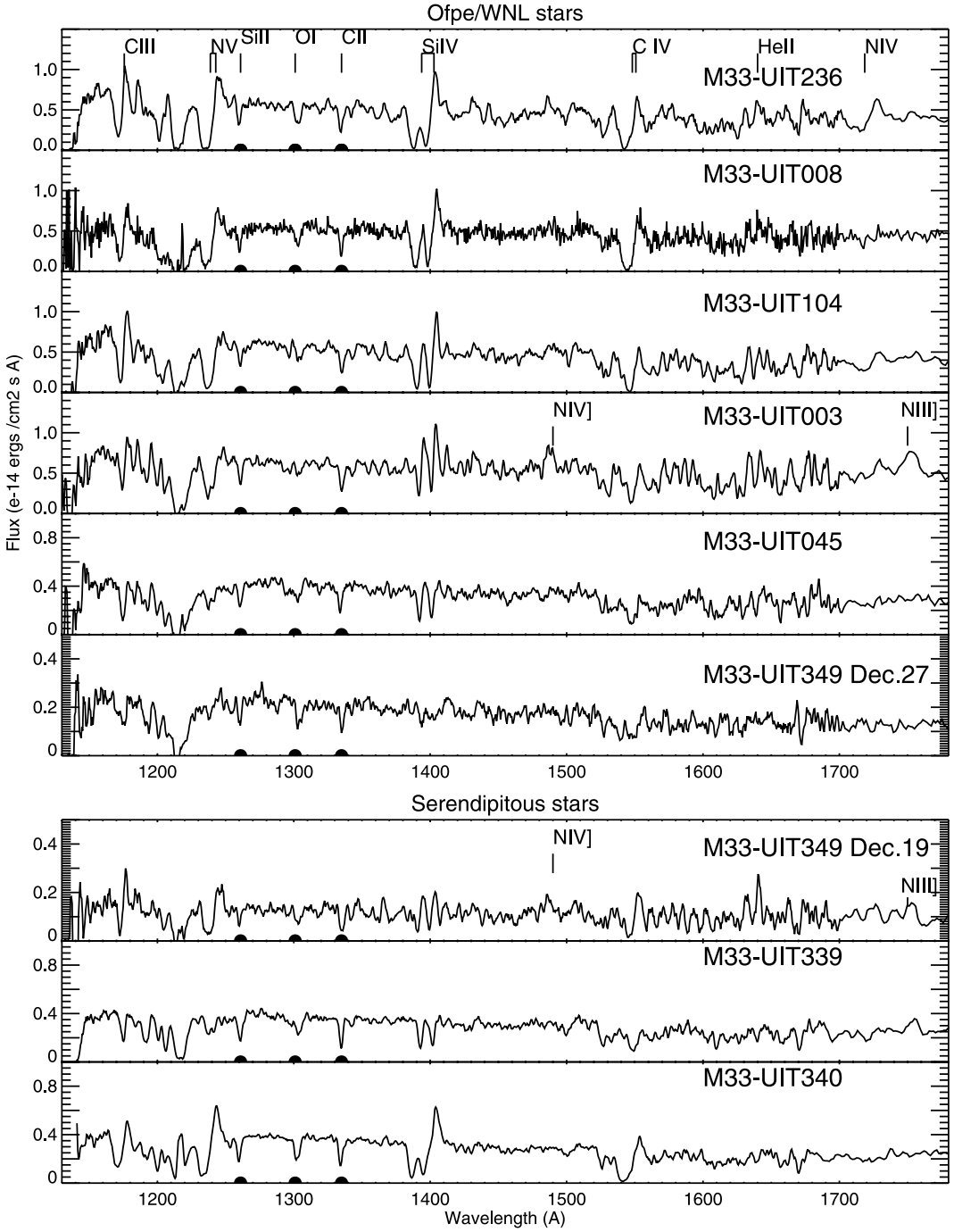

FIG. 1.—UV spectra in the short-wavelength range that contains the lines of interest: C III, C IV, N IV, N V, Si IV, and He II. The Ofpe/WN9 program stars are arranged by progressively decreasing strength of the UV wind lines. The spectra of the serendipitous stars (see text) are shown at the bottom. The strongest interstellar lines in this range, Si II λ1260, O I λ1301, and C II λ1335, are marked with a filled bubble at the bottom of the spectra. The strongest stellar features are also marked on the top spectrum.

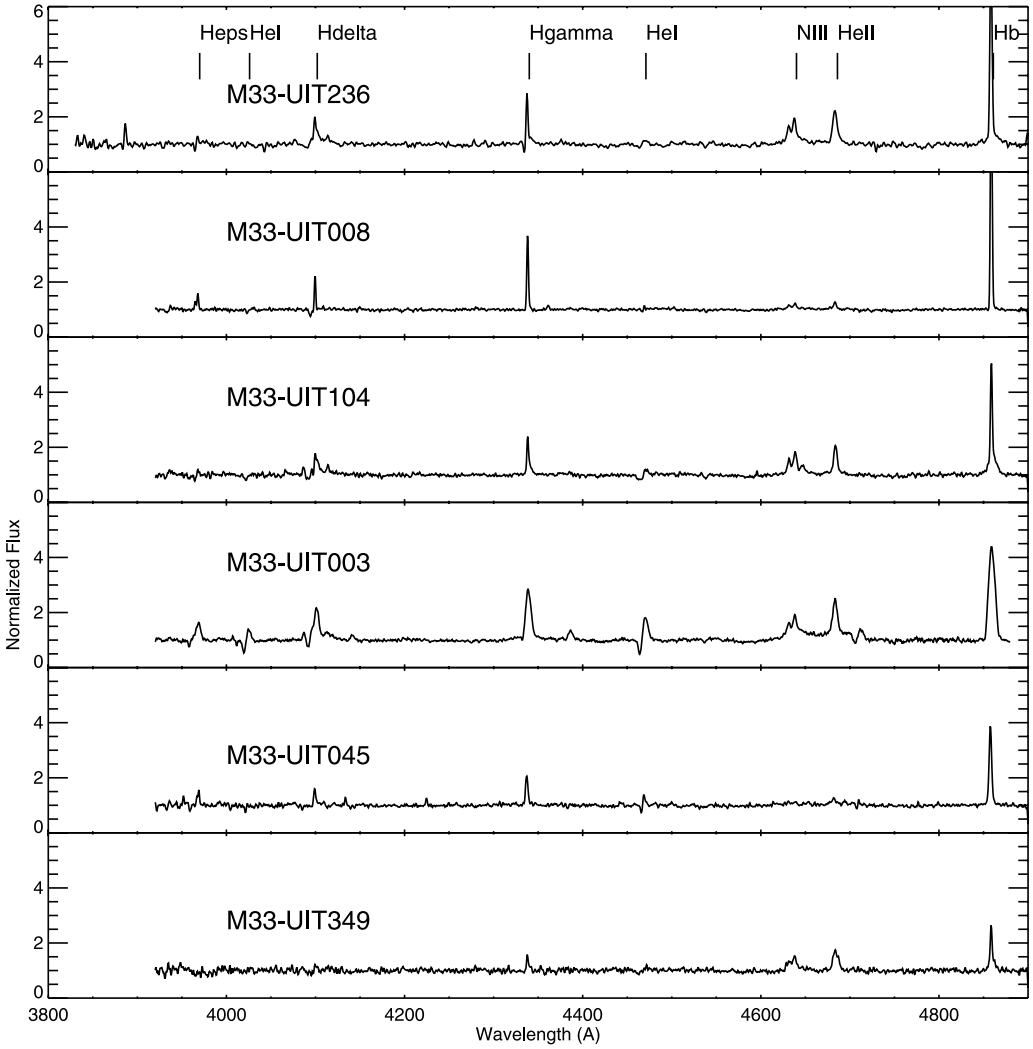

FIG. 2.—Optical spectra of the program stars (about 2 Å resolution; MBHS) are shown arranged in the same order as the UV spectra in Fig. 1. To facilitate appreciation of relative line strength, the spectra are normalized to the continuum and plotted on identical scale. The relative line strength does not match the progression seen in the UV lines, suggesting variability.

appropriate orientation. Its spectrum has a UV flux level comparable with the primary target but much stronger UV lines, in spite of the similar optical colors. Another serendipitous star was observed owing to failure of acquisition on a repeated observation of M33-UIT349.

Data from our previous ground-based photometry are compiled in Table 1. In the table we give the star name, coordinates, and V magnitude from the UIT sources list of MBHS. Also, for the position of every star we computed the deprojected galactocentric distance, using P.A. $= 22^\circ$ for the position angle of the semimajor axis of M33, an inclination of the disk $i = 54^\circ$, and a systemic velocity for M33 of $V_{\rm sys} = -180$ km s^{-1} (from Warner, Wright, & Baldwin 1973). Warner et al. (1973) also provide a model for the rotation of the M33 disk from H I measurements. We computed the expected disk velocity, projected along the line of sight, at the position of each star. Because the targets are likely to lie in the M33 disk, we used this velocity to shift the spectra to a rest-wavelength frame at the star. The position of the stellar lines indicates that this velocity correction is appropriate in all cases, although the difference from just using the M33 systemic velocity is not really appreciable at the resolution of our spectra. Both the galactocentric distance and the recessional velocity are also given in Table 1. Finally, the STIS data sets are listed.

2.2. *STIS Spectroscopy and Data Reduction*

The observations were completed over a long time span, because the *HST* entered a safe mode event just after our program (GO8207) began, and most of the observations were delayed because we missed the window for the desired orientation constraints. To assure homogeneous data quality and consistent flux calibration, we used the most recent on-the-fly calibration for all of the data after the program was completed.

The same observing pattern was repeated for each star: after target acquisition, a 24 minute long exposure was obtained with the STIS G230L grating (range: 1570–3180 Å; scale: 1.58 Å pixel^{-1}), followed by an 8 minute exposure in the same orbit with the grating G140L (range: 1150–1730 Å; scale: 0.60 Å pixel^{-1}). The whole subsequent orbit was devoted to a long (57 minute) G140L exposure. The total exposure times were therefore 3300 (G140L grating) and 1440 s (G230L grating) for every target. The STIS $0\farcs2 \times 52''$ slit was used. For target M33-UIT349, which is fainter than the others in the sample, we repeated this pattern twice,

TABLE 1

PROGRAM STARS AND THE STIS DATA

Star Name	R.A. (J2000.0)	Decl. (J2000.0)	D_{Gal} (Kpc)	V	$B-V$	$U-B$	STIS Data Sets (G230L and G140L)	M33 Velocity (km s^{-1})
				Ofpe/WN9 *S*tars				
M33-UIT236	01 33 53.58	30 38 51.8	0.4	18.08	−0.14	−0.84	O5CO04010, O5CO04020, O5CO04030	−165.7
M33-UIT008	01 32 45.38	30 38 58.6	6.0	17.67	−0.07	−1.01	O5CO05010, O5CO05020, O5CO05030	−145.4
M33-UIT104	01 33 27.22	30 39 09.1	2.1	18.03	−0.14	−0.91	O5CO03010, O5CO03020, O5CO03030	−147.5
M33-UIT003	01 32 37.70	30 40 05.7	6.8	17.44	0.01	−0.98	O5CO08010, O5CO08020, O5CO08030	−151.1
M33-UIT349	01 34 18.66	30 34 11.6	3.5	18.71	0.57	−0.83	O5CO07010, O5CO07020, O5CO07030	−153.0
M33-UIT045	01 33 09.10	30 49 54.5	5.8	18.02	0.00	−1.01	O5CO01010, O5CO01020, O5CO01030	−215.9
				Serendipitous Sources				
M33-UIT349-B	01 34 19.66	30 34 11.6	3.5	...	...	...	O5CO06010, O5CO06020, O5CO06030	−153.0
M33-UIT339	01 34 16.06	30 36 42.3	2.8	18.03	0.01	−0.83	O5CO02010, O5CO02020, O5CO02030	−173.4
M33-UIT340	01 34 16.04	30 36 38.0	2.8	18.42	−0.04	−0.81	O5CO02010, O5CO02020, O5CO02030	−173.4

NOTE.—Units of right ascension are hours, minutes, and seconds, and units of declination are degrees, arcminutes, and arcseconds.

aiming at doubling the total time and achieving a signal-to-noise ratio (S/N) comparable with those of the other sample objects. The two sets of observations were taken about a week apart (2000 December 19 and 27). The spectra are significantly different on the two dates, both in flux level and wind lines, as can be seen in Figure 1. After examining the STIS CCD50 acquisition images, we discovered that the intended target (M33-UIT349) was actually observed on December 27, while a nearby star was centered in the aperture on December 19, during the fine-centering stage, although the right target was exactly centered (on the same pixel) after coarse acquisition on both dates, as shown in Figure 3. We measured photometry on both dates on the STIS CCD acquisition images: the two stars are equally bright in the CCD50 filter. In addition, the target (M33-UIT349) appears slightly elongated in the acquisition images (Fig. 3), but it is not clearly resolved into multiple sources. A cut of the long-slit two-dimensional spectra along the spatial direction, obtained by summing several columns across the wavelength dispersion (Fig. 4), shows a hint of a faint extension in M33-UIT349 spectrum (December 27; data sets O5CO07010, O5CO07020, and O5CO07030), although the two peaks, or asymmetric intensity profile, may just be an effect of the low count rate. The STIS MAMA spatial scale is $0\farcs025$ pixel^{-1}, and the width of the entire spectrum (see Fig. 4) is about 10 pixels, or $0\farcs25$, with the two brightest components less than $0\farcs1$ apart. Therefore, it appears that although the object is not resolved into multiple stars in the STIS CCD, which has a factor of 2 lower resolution than the MAMA, there may be some (marginal) extra light entering the STIS slit from other fainter sources. The spectra are centered in the *y*-direction (perpendicular to the dispersion) in the nominal position. On the basis of the elongation seen on the finding chart and the two apparent peaks in the spectrum intensity profile, we can speculate, could the object be a binary (multiple?) system, or is there a chance superposition of a faint source? A separation of $\leq 0\farcs1$ at the distance of M33 (840,000 pc; Magrini et al. 2000) would correspond to ≤ 0.4 pc, which is extremely large for a bound binary. An additional source seems to be excluded by the quantitative modeling of the spectra.

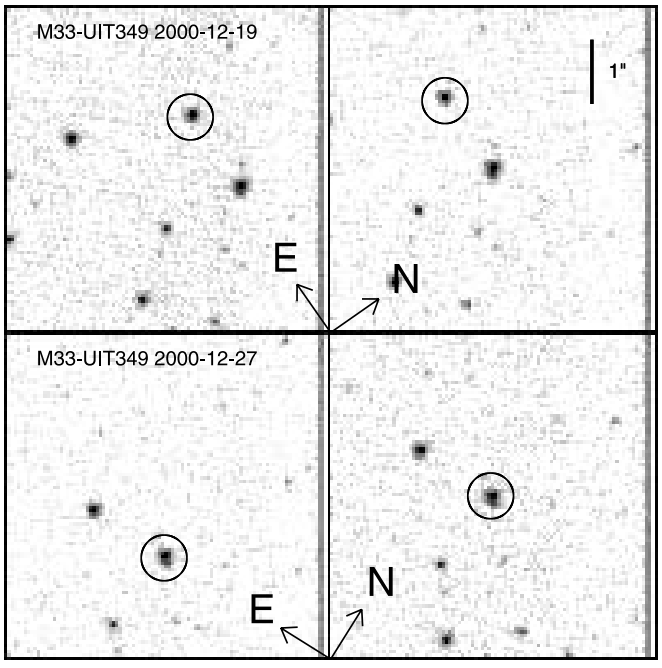

FIG. 3.—Acquisition images of M33-UIT349. *Left:* Before centering; *right:* after coarse acquisition centering. Note that the orientation is different on the two dates (P.A. $= 54\fdg65$ on December 19 and P.A. $= 31\fdg64$ on December 27). The target was acquired and perfectly centered in the coarse stage on both dates; however, on December 19, during the fine acquisition, there was a jump and another star of equal brightness (*circled*) was put in the slit.

We will call the serendipitous star that was in the slit on December 19 M33-UIT349-B in Table 1. In the acquisition image, it is just $1\farcs33$ east of the target, and thus the coordinates given in Table 1 are relative to the ground-based coordinates of the source ($+0\fs10$ in right ascension). Most likely, the ground-based coordinates of M33-UIT349 were an intermediate position between the two sources, whose separation of $1\farcs3$ is not resolved in the ground-based image and is comparable with the coordinate accuracy. The two stars can be uniquely identified by their relative positions and our finding chart (Fig. 3).

For every target star we examined the two G140L exposures taken in subsequent orbits and found that they perfectly match in absolute flux and that the strong line features reproduce very well—in spite of the very different S/Ns, due to the different exposure time. Also, we verified that the G230L and G140L fluxes match in the wavelength region of overlap. With the exception of M33-UIT339 (see below), we then combined the two G140L exposures, taking into account the different exposure times, to obtain the maximum possible total S/N over the range. The STIS flux calibration is expected to be accurate for sources in the broad $2''$ wide slit to 2% (Bohlin 2000; Bohlin, Dickinson, & Calzetti 2001). For the $0\farcs2$ slit used in this program, photometric precision of one wavelength with respect to a distant wavelength is 4.5% rms (Bohlin & Hartig 1998). There are no known nonlinearities in the response of the STIS MAMA detectors. However, additional uncertainties arise from the Poisson counting statistics and from possible errors in background subtraction for the faintest sources.

An additional target, M33-UIT339, was included in our program GO 8207 since it appeared to be an Hα emission-line source; however, it was not subsequently classified as an Ofpe/WN9 star. With an appropriate orientation, the STIS long slit centered on M33-UIT339 included also M33-UIT340, separated by about $4''$. The pipeline automatic extractions for the two G140L spectra, taken in subsequent orbits, are centered on the two different stars, respectively; therefore, the extracted spectra from the archive should *not* be used. The automatic pipeline extraction centered the extraction slit on the target in one case (data set O5CO03020) and on the serendipitous star in the other case (data set O5CO03030). Therefore, we manually reextracted the spectra of both stars in all three exposures (two G140L and one G230L) and co-added them separately. While there is no acquisition image for the second orbit (only re-acquisition of previous guide stars was performed), we did obtain a parallel WFPC2 image with the same filter (F170W) in each orbit, as well as with different filters. Our F170W WFPC2 images with $0\farcs1$ resolution show that there is no shift between the two pointings down to the pixel level. The continuum level is the same over most of the G140L range, but the wind features are completely different for the two stars (Fig. 1).

The spectra of the serendipitous stars are shown in Figure 1 for completeness and for clarification of all acquisition and multiple-source issues for potential archive users. They will be analyzed separately.

Because the targets were selected from ground-based photometry and spectroscopy, we examined all the STIS acquisition images to check for multiplicity that might be revealed at the

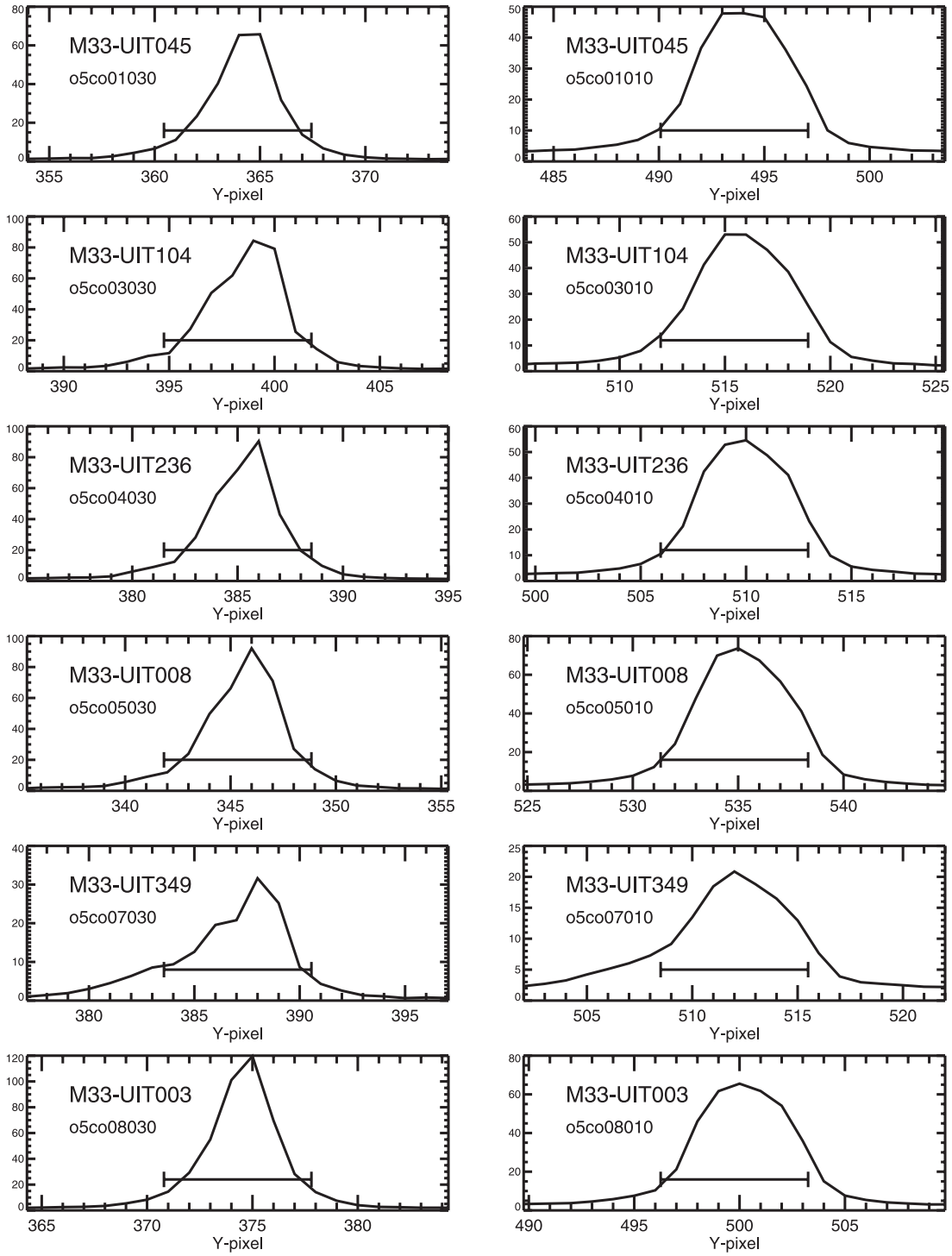

FIG. 4.—Intensity profile in the spatial direction for the G140L (*left*) and G230L (*right*) spectra for all the program stars. The profile is the sum of 301 columns around the center of the image. The data shown for M33-UIT349 are from the December 27 observations, when the correct target was observed.

HST/STIS imaging resolution but not in the ground-based data. All targets appear pointlike.

3. ANALYSIS OF THE UV SPECTRA

3.1. *UV Line Morphology*

The short wavelength (<1750 Å) portion of the spectra for all the program stars and the serendipitous stars is shown in Figure 1. This wavelength region is richest in lines from the stellar wind (and the interstellar medium). The main wind lines are shown in detail in Figure 5, where their extent in velocity (largely varying across the sample) can be appreciated. The spectra are arranged from top to bottom of the figures in a progression of decreasing strength of the UV lines and decreasing wind velocity (width of the P Cygni absorption). Previous ground-based spectroscopy from MBHS also showed a range of line strengths within the sample. However, the progression is different from what the recent UV spectra indicate. The optical spectra from MBHS are shown in Figure 2. For example, M33-UIT008 was a weak liner in the optical

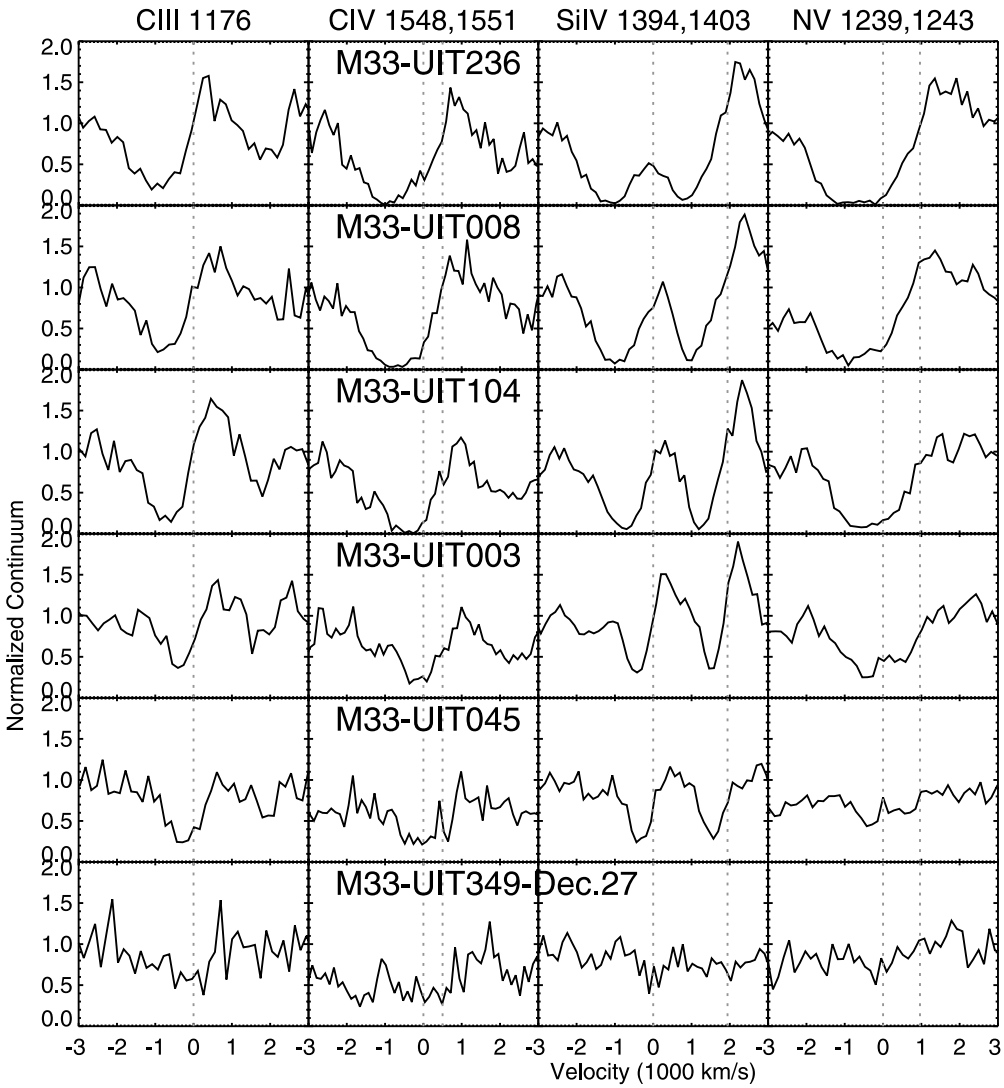

FIG. 5.—Four strongest UV wind lines are shown in velocity scale (1000 km s^{-1}) for the Ofpe/WN9 program stars. Vertical dotted lines indicate the rest positions of the transitions. The recession velocity of each star (Table 1) has been removed. From top to bottom, the lines show a progression of decreasing strength and width (i.e., decreasing wind terminal velocity). The effect is especially evident in the Si IV doublet, where the two components are more separated in wavelength (while the C IV and N V doublets are always blended in velocity). [*See the electronic edition of the Journal for a color version of this figure.*]

spectra but displays some of the strongest UV features in the STIS spectra. On the other hand, M33-UIT349 has fairly strong optical lines (Fig. 2), but not in the UV spectra. As another example, M33-UIT045 has weak lines both in the old optical spectra and in the UV spectra.

The UV line strength progression indicates a range of $T_{\rm eff}$ (luminosities) and mass-loss rates among the sample. It is difficult to relate the progression to an evolutionary sequence, because the relative line strengths of the optical spectra ($\approx$1993–1995) and the recent (2000–2001) UV spectra differ, suggesting variability. One stellar parameter that can plausibly vary on very short timescales is the mass-loss rate, if these objects are single stars. Or are they evolved binaries? The quantitative spectral modeling described below is aimed at clarifying the evolutionary status by measuring the stellar parameters.

3.2. *Non-LTE Modeling with WM-BASIC*

We performed detailed quantitative modeling of the spectra with the WM-BASIC code (Pauldrach, Hoffmann, & Lennon 2001). The code solves the wind hydrodynamics equations for specified parameters and includes non-LTE metal line blanketing in spherical geometry. It also allows us to include the effects of shocks (from clumps) on the wind ionization in the radiative transfer calculations, which are extremely important for a correct modeling of hot massive stars (e.g., Bianchi & Garcia 2002, 2003). Below we discuss the determination of the physical parameters for each individual star and how the uncertainties were estimated. More discussion on the uncertainties can be found in § 4. The parameters from the best-fit models are listed in Table 2. The process is quite complex, given the many physical parameters that affect the emerging spectrum. The analysis of the first object is thus described in detail as a sample case. The effects of the physical parameters on the emergent spectrum are similar for the other objects. Initial guesses for the terminal velocities were made by measuring the maximum extent of the P Cygni profile absorptions, which largely varies across the sample, as can be appreciated (on an expanded scale and independent of any modeling) in Figure 5.

3.2.1. *M33-UIT236*

The UV spectrum of this object indicates that it might be the hottest of the sample and that it has a high mass-loss rate,

TABLE 2
Derived Stellar Parameters

Star Name	$E(B-V)$ (mag)	V_∞ (km s^{-1})	$T_{\rm eff}$ (K)	log g	$L/L_\odot$	$R/R_\odot$	$\dot{M}$ ($M_\odot$ yr^{-1})	$L_X/L_\odot$	M ($M_\odot$)	[C]/[C$_\odot$]	[N]/[N$_\odot$]	C/N (by mass)
M33-UIT236	0.10	1950 ± 150	33,000 ± 1500	3.2	5.67	21	8E−6	−7.5	26	0.05	10	0.02
M33-UIT008	0.08	1950 ± 150	32,000 ± 1000	3.2	5.66	22	4E−6	−7.75	28	0.05	10	0.02
M33-UIT104	0.09	1600 ± 150	31,000 ± 1500	3.2	5.61	22	3E−6	−8.0	28	0.50	2	0.90
M33-UIT003	0.07	1000 ± 120	30,000 ± 1500	3.2	5.55	22	2E−6	−10	28	0.05	10	0.02
M33-UIT045	0.10	950 ± 100	30,000 ± 1500	3.2	5.47	20	5E−7	−9.5	23	0.5	0.1::	17::
M33-UIT349	0.11	1700:	27,000 ± 2000:	3.0:	5.28:	20:	1E−8:	−7.0:	15:	0.5:	2:	0.90

because it has the strongest UV wind lines. We ran a grid of WM-BASIC models, with initial parameters covering a range of values for $T_{\rm eff}$, luminosity, and mass-loss rate inferred from a wider grid computed for other purposes. We computed synthetic model spectra for both solar and LMC-type metallicities and then also varied individual abundances of the CNO elements. In Table 2 we give the resulting stellar parameters and their uncertainty range, and here we discuss how they were constrained.

Before we discuss the strong P Cygni profiles that primarily constrain the main stellar parameters, we note that all models of the initial grid computed for LMC-type metallicity ($z = 0.008$) are "flatter" than the observed spectra in some spectral regions that contain no single strong lines but rather a multitude of fainter lines, mainly from Fe III and Fe IV transitions (e.g., from 1420 to 1500 Å). In these regions, the emerging flux in the low (LMC-type) metallicity models is close to a pure continuum, while the observed spectrum definitely shows shallow but significant depressions. These can be reproduced better in models with solar metallicity ($z = 0.02$). A precise determination of z is not possible. Therefore, we adopted solar metallicity in the subsequent computation of the finer grid that includes the best-fit adopted solutions, discussed hereafter. The result is not surprising given the metallicity gradient in M33 and the fact that M33-UIT236 is relatively close to the galaxy center. The model spectra are sensitive to this effect only for large wind velocities.

The STIS spectrum of M33-UIT236 (Fig. 1) shows strong P Cygni profiles of both Si IV and N V, as well as a strong C IV $\lambda\lambda$1548, 1551 doublet and C III multiplet around 1174 Å. To reproduce the observed strength of both N V and Si IV consistently, we need to take into account the X-rays produced by shocks in the wind as a relevant ionization process. Because there is no prior information, to our knowledge, about soft X-ray emission from these objects, we tried a range of values that would be appropriate for early-type luminous stars as observed, e.g., in our Galaxy (e.g., Bianchi 1982a, 1982b; Bianchi & Garcia 2002,). We found that for $T_{\rm eff} = 32,000$ K or lower, $L_X/L_\odot \approx -7$ is appropriate for reproducing the strength and shape of the N V doublet and the other "hot" transitions relative to the lines from lower ionization potential stages such as Si IV. A lower X-ray luminosity of $L_X/L_\odot = -7.5$ is found to be adequate at a higher $T_{\rm eff}$ (34,000 K). The Si IV $\lambda\lambda$1394, 1403 doublet, as well as N IV λ1718, is not very sensitive to the effect of shocks but is instead very sensitive to $T_{\rm eff}$ (especially in the range 34,000–30,000 K) and to the mass-loss rate. He II λ 1640 is very sensitive to the mass-loss rate in this temperature regime and thus cannot be used to constrain the helium abundance. The *relative* strength of the C IV to C III lines is again best reproduced by models between $T_{\rm eff} = 32,000$ and $T_{\rm eff} = 34,000$ K. However, both of these C lines are always too strong for all parameter combinations which can reproduce the overall spectral features in the models with solar abundances. We have therefore progressively decreased the C abundance (and changed correspondingly the abundance of N and O as expected in different evolutionary scenarios) and finally achieved a consistent fit of all the strongest wind lines with carbon 20 times less abundant than the solar value and nitrogen 10 times more abundant. These values correspond to the abundances predicted by evolutionary models for, e.g., a star with initial mass of ≈30–50 $M_\odot$ reaching the WNL stage. The evolutionary models also predict oxygen to be underabundant by a factor of 10 with respect to solar and He/H of up to 0.5 for evolved massive objects reaching such C and N abundances (e.g., Maeder 1987; Maeder & Meynet 1994; Meynet & Maeder 2000, 2003). We thus also adopted $[{\rm O}] = 0.1$ the solar value for consistency with our findings of the C and N abundances, although there are no strong oxygen lines in the range covered by our STIS spectra for stars in this temperature range to directly measure the oxygen abundance.

We varied He/H from 0.1 to 0.5 (by number), and in both cases we can achieve an acceptable fit of the overall spectrum by slightly tuning the other parameters. Best fits are obtained with $T_{\rm eff} = 32,000$ K if He/H = 0.1 and with $T_{\rm eff} = 34,000$ K for He/H = 0.5. Changing the helium abundance affects not only the strength of the He II λ 1640 but the relative strengths of other lines. Therefore, we consider the actual helium abundance a source of uncertainty and adopt the above range for $T_{\rm eff}$.

Once the *strength* of all P Cygni lines in the spectrum was matched by the models and the acceptable ranges were constrained, we fine-tuned the trough of the absorptions, especially for the Si IV doublet, which is partly resolved. We varied both the terminal velocity and the rotational velocity. While the terminal velocity significantly affects the separation of the two absorption components of the Si IV doublet and its uncertainty range is easily determined (see Fig. 5 and Table 2), rotational velocities of $V \sin i = 60$ km s^{-1} and twice as high $V \sin i = 120$ km s^{-1} were tested in the model calculations: the change only slightly affects the shape of the absorption troughs. This analysis is not as sensitive to this parameter ($V \sin i$) as the optical photospheric lines, since lines at UV wavelengths are mainly produced in the wind thus broad and asymmetric, and the STIS spectra resolution is too low for this purpose. The fit of the C III and Si IV lines, favors the high rotation. Again, a quantitative determination of this parameter is not possible; we can only infer from the comparison an indication of possible high rotation.

All the best-fit models shown are computed with log $g = 3.2$. The low gravity value was initially driven by the intention

to compute models with reasonable mass/radius/luminosity values for this type of stars. We then tried higher gravities and obtained worse line fits. Note the good match of both the absolute flux values (a further confirmation that our choice of the radius in the best-fit models is adequate) and of the slope of the spectrum, which independently confirm the temperature derived above by fitting the line strengths and the extinction value (which is also consistent with the previous work of MBHS). Because the spectral slope depends on $T_{\rm eff}$ (and reddening) and the absolute flux depends on R^2 and $T_{\rm eff}{}^4$, the overall match to both the line profiles and the absolute flux level confirms the consistency of the parameters derived from our analysis.

The derived C/N ratio (by mass) of 0.02 is significantly lower than the cosmic value (4.8) and in the range of the WNL-type stars (see, e.g., Massey 2003). The C/N value is consistent, according to the stellar evolution calculations of Maeder (1987), Maeder & Meynet (1994), and Meynet & Maeder (2000, 2003) with the surface abundances of a massive star during the transition stage from B supergiant to WNL. The current mass, $T_{\rm eff}$, and luminosity derived from our spectral modeling for M33UIT 236 agree with the evolutionary models for an initial mass of about 50 $M_\odot$.

3.2.2. *M33-UIT008*

If we superpose the spectrum of this star to the previous one (M33-UIT236), the two spectra, normalized to the respective continua, are basically identical except for much weaker nitrogen lines in M33-UIT008. In particular, the C IV and C III lines are identical, and so is the Si IV doublet, except for a clearer separation of the two absorption components, indicating slightly lower terminal velocity or mass loss in M33-UIT008. He II λ1640 is also identical. However, the N IV and N V lines are both significantly weaker than in the previous star. We attempted to explain this difference by either a lower nitrogen abundance or a lower $T_{\rm eff}$ or $\dot{M}$. In our grid of models for solar CNO abundances, the N IV λ1720 line becomes very weak (comparable with the one seen in the M33-UIT008 spectrum) when $T_{\rm eff}$ is cooler than 28,000 K for mass-loss rates of $3-5\times 10^{-6}$ $M_\odot$ yr^{-1}, but the strength of this line also decreases significantly with decreasing mass-loss rate. However, these models with lower $T_{\rm eff}$ produce too much Si IV and too little C III with respect to the observed spectrum if we keep the other parameters similar to those of M33-UIT236, including the CNO WNL-type'' abundances. In short, a good fit of the other lines cannot be achieved at such low $T_{\rm eff}$.

The strength of the N V doublet significantly decreases in models with lower $L_{\rm X}/L_\odot$; however, N IV is practically unaffected by this change and the Si IV doublet is significantly enhanced. Therefore, varying this parameter does not produce a good fit either.

Because both N IV and N V transitions are weaker in M33-UIT008 than in M33-UIT236 but the spectra are otherwise identical, we computed models with the same parameters as the best fit of M33-UIT236 but lowered the nitrogen abundance from WNL values down to the solar value. This produces slightly lower (not low enough) nitrogen lines but enhances the Si IV and C IV emissions enormously. Probably because we keep other parameters (such as mass-loss rate) the same, the opacities are redistributed. We also tried to decrease the mass-loss rate and alter other parameters, including different combinations of abundances and the amount of shocks.

The best fit, in terms of the relative line strength and match to the flux below 1700 Å, is achieved with the parameters given in Table 2. The results indicate that the main difference with respect to M33-UIT236 is a lower mass-loss rate.

We caution that Bianchi & Garcia (2002) and M. Garcia & L. Bianchi (2003, in preparation) encountered some difficulties in fitting weak N V lines in Population I Milky Way stars with the WM-BASIC code and that better matches could be achieved in some cases using Hillier's CMFGEN code, although the resulting stellar parameters were not changed (e.g., Bianchi, Garcia, & Herald 2003; L. Bianchi, M. Garcia, & J. Herald 2003, in preparation). Therefore, the derived abundances, in particular of N in this case, must be taken as indicative, as stressed in the previous section.

3.2.3. *M33-UIT104*

The *line* spectrum suggests lower wind velocity and a lower stellar temperature than the previous stars examined, the ''cooler'' transitions (C III and N IV) being enhanced and the higher ions (N V and C IV) weaker. A similar effect on the line strength may to some extent be produced by a lower amount of X-rays from shocks. All these effects were quantified by the modeling (Table 2). A C III line, visible as a small but detectable absorption in the emission of N V, is the most unambiguous indication of $T_{\rm eff}\leq 32{,}000$ K according to our grid of models (see Bianchi & Garcia 2002), at least for solar abundances. Therefore, this line provides a strong constraint on $T_{\rm eff}$.

In this $T_{\rm eff}$ regime, the C III 1175 Å line becomes much more sensitive to the C abundance than to the mass-loss rate (while C IV is saturated so rather insensitive to all parameters). This is very fortunate because it allowed us to constrain one parameter (the C abundance) relatively independently of the other ones in this case. Along the stellar evolution, the C depletion develops concurrently with the N enrichment (according to Maeder 1987); therefore, we tried different abundance ratios for C and N, corresponding to a typical predicted evolutionary sequence. The best fit is shown in Figure 6 and was achieved with [C] = 0.1 times solar and [N] = 2 times solar. In mass fraction, this means C/N = 0.9.

Again the match to both the line strength and to the absolute flux level, as well as the continuum shape, is very good shortward of 1700 Å.

3.2.4. *M33-UIT003, M33-UIT349, and M33-UIT045*

Continuing toward progressively weaker P Cygni profiles and lower terminal velocities, M33-UIT003, M33-UIT045, and M33-UIT349 (December 27) show a smooth decrease in the lines of Si IV and C IV, compared with the previous targets. Instead, the N V λ1240 doublet abruptly disappears in the spectra of M33-UIT045 and of M33-UIT349. In modeling the spectrum of M33-UIT045, it has been impossible to obtain a synthetic spectrum that matches the line features and the absolute flux, with nitrogen abundance solar or higher. The best-fit spectrum (shown in Fig. 6) was obtained by lowering the nitrogen abundance by a factor of 10 with respect to solar. A nitrogen underabundance in such evolved massive star is hard to explain and extremely suspicious. Again, we caution that model calculations may be less reliable for such extreme parameters than for the previous cases.

Similarly to M33-UIT045, it has been extremely difficult to produce a synthetic spectrum without N V to match the observed spectrum of M33-UIT349. The fit was achieved with an extremely low mass-loss rate, about 2 order of magnitude

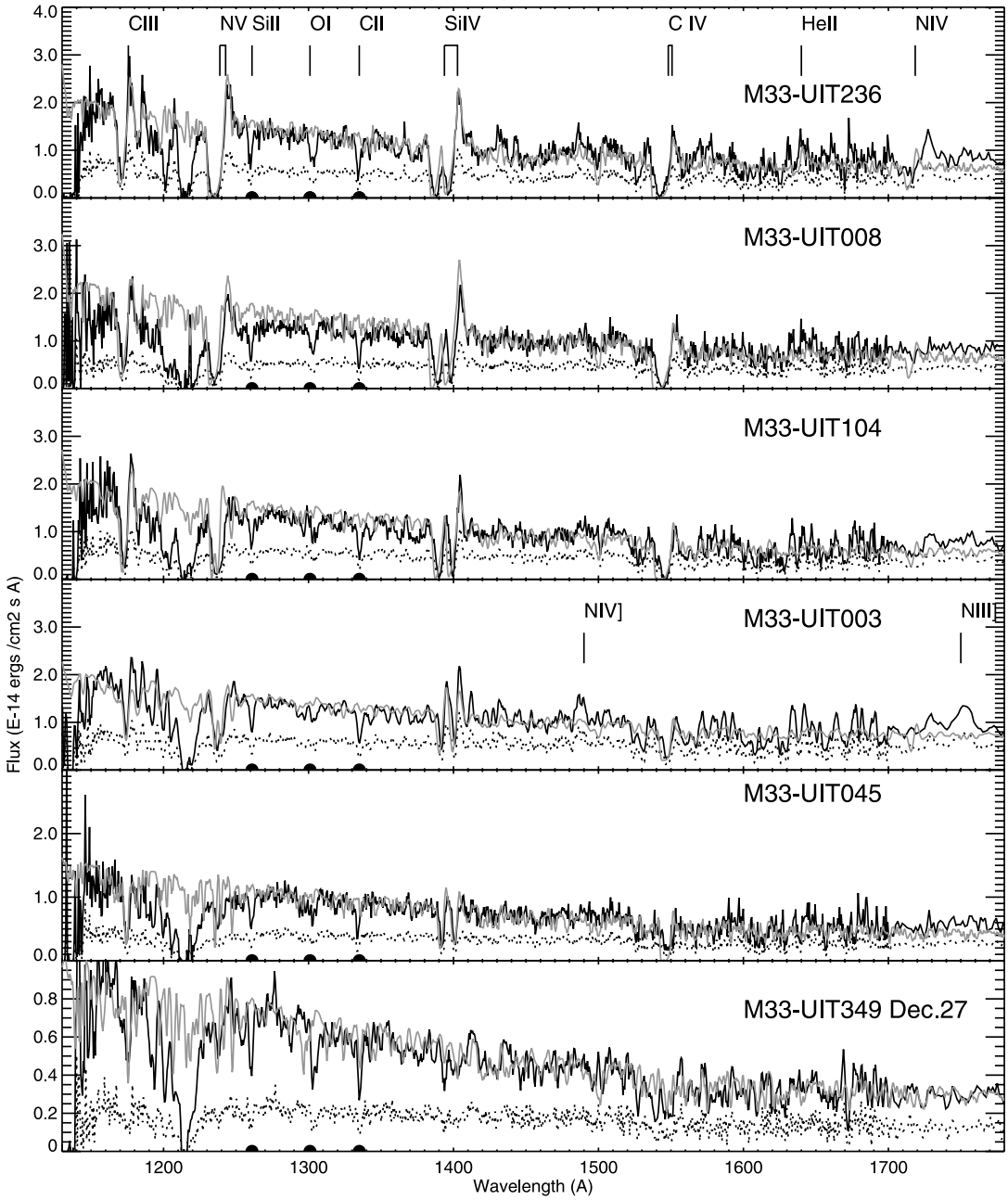

FIG. 6.—STIS spectra (*solid line*), dereddened for the amount of extinction given in Table 2, and the best-fit models (*light gray*) computed with WM-BASIC. The model parameters are compiled in Table 2. The dotted line is the observed spectrum with no dereddening, to illustrate the sensitivity of our modeling to even such small reddening amounts. The range below 1800 Å is shown, where all the strong stellar wind lines are. The strongest interstellar lines in this range, Si II λ1260, O I λ1301, and C II λ1335, are marked with a filled bubble at the bottom of the spectra. In the spectrum of M33-UIT003 two broad emission features are seen, near 1490 and 1750 Å. There are a number of N IV] and N III] intercombination lines around those wavelengths respectively. The emission is probably not of stellar origin. [*See the electronic edition of the Journal for a color version of this figure*.]

lower than the other stars in the sample. The result is consistent with the fact that the typical wind lines in the UV spectrum are almost absent. However, the low mass-loss rate is surprising since this star has photospheric parameters not too different from the rest of the sample. We must keep in mind that additional faint sources may contribute—although marginally—to the spectrum, but they are not resolved nor confirmed. It is also puzzling that the wind lines in the M33-UIT349 spectrum seems *wider* rather than narrower compared to the spectra with stronger lines. Typically, a progression from stronger to weaker P Cygni profiles (i.e., decreasing mass loss) also corresponds to decreasing wind velocities, as it evident, e.g., in the sequence of spectra in Figures 1 and 5 (*top to bottom*). The large velocity may suggest a physical binary, i.e., two stars with high ($\approx$1000 km s^{-1}) velocity relative to each other, both having weak lines. Or, more simply, the fact that the lines are so weak (and the limited S/N) prevents the resolution of blends and makes the analysis inconclusive in this case.

Finally, for two "weak-lined" spectra, modeling was achieved with a carbon underabundance (with respect to solar) of a factor of 2, not 20, as for the hotter stars with stronger winds and lower mass values. The derived parameters $T_{\rm eff}$, $L_{\rm bol}$, and mass, are again consistent with the evolutionary models of Maeder, since lower mass stars produce less

enhancement of N and less depletion of C than more massive stars.

Looking at the absolute flux level and slope at longer wavelengths (Fig. 7), we note a slight mismatch between the model and observed spectra for M33-UIT008, M33-UIT045, and M33-UIT003. While the best-fit model reproduces well the continuum and all the lines in the shorter wavelengths range (where the flux from the hot star dominates), the slope of the entire observed spectrum cannot be matched perfectly by any single-star model for any combination of reddening (using known reddening types). The mismatch between model and observed spectra, however, is of the order of $0.1 - 0.2 \times 10^{-14}$ ergs cm^{-2} s^{-1}, or $\approx$up to 5% beyond $\approx$1500 Å, and is thus comparable with the calibration uncertainty. The flux level and the line spectrum are matched well in the short-wavelength range, pointing to a consistent and plausible model fit for the hot star. In the finding chart produced from the STIS CCD acquisition image and the spectral intensity cuts shown in Figure 4, no extra faint components can be clearly resolved. Therefore, the mismatch could indicate either an unresolved chance superposition of a fainter cooler star (statistically unlikely), a faint binary component with separation less than $\approx$0.2 pc (unresolved), or an UV extinction slightly different from the types known so far in the Milky Way or the LMC (see next section). The level of mismatch, is however, of the order of the calibration accuracy (see § 2.2.); therefore it could just be an instrumental effect.

4. DISCUSSION AND CONCLUSIONS

We analyzed STIS Ultraviolet spectra of six Ofpe/WN9 stars in M33. Previous optical spectra of our sample (MBHS) showed a progression from "weak-lined" slash stars, similar to BE 470 in the LMC (with strong P Cygni, He I, and Balmer emission but very weak N III $\lambda\lambda$4634, 4642 and He II λ4686) to "strong-lined" slash stars, similar to BE 381 in the LMC (with strong N III and He II). The UV line spectra show a progression (Fig. 1) of line intensities that does not correlate with the earlier optical spectra (Fig. 2), suggesting possible variability on a short timescale (years) of the mass-loss rate.

One target, M33-UIT349, was observed twice, 8 days apart, but successfully only on December 27. Its spectrum seems to include a very faint extension (Fig. 4), separated spatially by less than 0.″1 (thus, if physically associated, by less than 0.4 pc), but the source is not resolved into separate components at the STIS CCD resolution (Fig. 3). In any case, the apparent secondary component has negligible flux with respect to the main source (Fig. 4), as confirmed by the good fit to the spectral distribution. The spectrum shows extremely weak wind lines.

For three stars (half of the sample) we find C/N = 0.02 by mass, consistent with predictions from stellar evolution models for an evolved massive star (initial mass $\approx$40–50 $M_\odot$) in the phase transitioning from blue supergiant to WNL (i.e., toward the W-R stage) at constant luminosity in the H-R diagram. The other physical parameters ($T_{\rm eff}$, mass, and luminosity) are also entirely consistent with the scenario of massive stars approaching the WNL stage (Maeder 1987; Maeder & Meynet 1994; Meynet & Maeder 2000, 2003). It must be kept in mind that the available spectroscopic range provides several wind lines but no photospheric lines; therefore, derivation of abundances is not very accurate since wind line strengths depend also on the mass-loss rate and other factors. However, the consistency of the entire modeling (lines, absolute flux, and velocity) supports the results as quite reliable, and all the parameters indicate a consistent evolutionary picture. For the other three stars, C was found to be (by number) only about half the solar value. For M33-UIT104, the analysis indicates N to be overabundant by a factor of 2, i.e., C/N = 0.9 by mass. For the other two stars with extremely weak lines, the nitrogen abundances and the overall modeling is much more uncertain, for the reasons explained in the previous section. Either these stars are in an earlier evolutionary stage, evolving off the zero-age main sequence, still toward lower values of $T_{\rm eff}$, or their progenitors have lower initial masses (by comparison with Maeder's evolutionary calculations). Variability of the mass-loss rate is also possible, as mentioned, complicating the interpretation.

Studies of coeval clusters in the Milky Way (Massey et al. 2001) and the Magellanic Clouds (Massey, Waterhouse, & DeGioia-Eastwood 2000) suggest that LBVs are descended from the most massive stars (>90 $M_\odot$). The two Ofpe/WN9 stars in their sample, however, come from stars of much lower mass, greater than 25–35 $M_\odot$, calling into question the evolutionary link between LBVs and Ofpe/WN9s. The range of progenitor masses inferred by comparing our derived current masses, abundances, $T_{\rm eff}$, and luminosities with evolutionary calculations ($\approx$30–50 $M_\odot$) is consistent with their findings. On the other hand, a link between LBVs and Ofpe/WN9 has been observationally established in the cases, e.g., of AG Car, R127, S61, and S119 (Stahl 1987; Stahl et al. 1983; Pasquali et al. 1999; Nota et al. 1995), although these studies do not provide enough statistics to quantify the correlation in terms of evolution. Langer, Heger, & Fliegner (1998) and Lamers et al. (2001) discuss the effect of stellar rotation on the evolution of massive stars and show that rotation "extends" the occurrence of the LBV phase to lower progenitor masses.

One important parameter, the mass-loss rate, varies from 8×10^{-6} to 2×10^{-6} $M_\odot$ yr^{-1} among the first four stars in Table 2, which appear to have similar masses (within the uncertainty of our analysis) but a range of temperatures. The uncertainties of the mass-loss rates are less than 30% according to our model calculations.

Although the difference in $T_{\rm eff}$ in our sample covers a fairly narrow range and the sample is numerically limited, there is a trend of mass loss increasing as the star evolves toward the W-R stage and becomes hotter. The mass-loss rate increases with luminosity (e.g., Bianchi & Garcia 2002; Nugis & Lamers 2000; Vink, de Koter, & Lamers 2001), but the small range of luminosity variation among the sample does not explain the large mass-loss rate spread (see below).

The values of $\dot{M}$ that we derive for the "strong-line" stars (the first four in Table 2) are lower than the high mass-loss rates of W-R stars and higher than the mass-loss rates expected for O stars with similar parameters. Maeder's evolutionary models assume an average $\dot{M} = 4 \times 10^{-5}$ $M_\odot$ yr^{-1} for WNL stars, and the Nieuwenhuijzen & de Jager (1990) parameterization for the earlier stages (this parameterization is based on a compilation of observed mass-loss rates). Our mass-loss rates are also lower than Nieuwenhuijzen & de Jager (1990) parameterization which, for the physical parameters given in Table 2, would predict for the first four stars of the sample $\dot{M}$ between 2.1 and 1.5×10^{-5} $M_\odot$ yr^{-1}. Recent works have revised the mass-loss rates for W-R stars, taking into account "clumping" in the wind. These mass-loss rates are generally lower than earlier determinations, of the order of $\geq 1 \times 10^{-5}$ $M_\odot$ yr^{-1} for WN-type stars of comparable luminosities to our targets (Nugis & Lamers 2000;

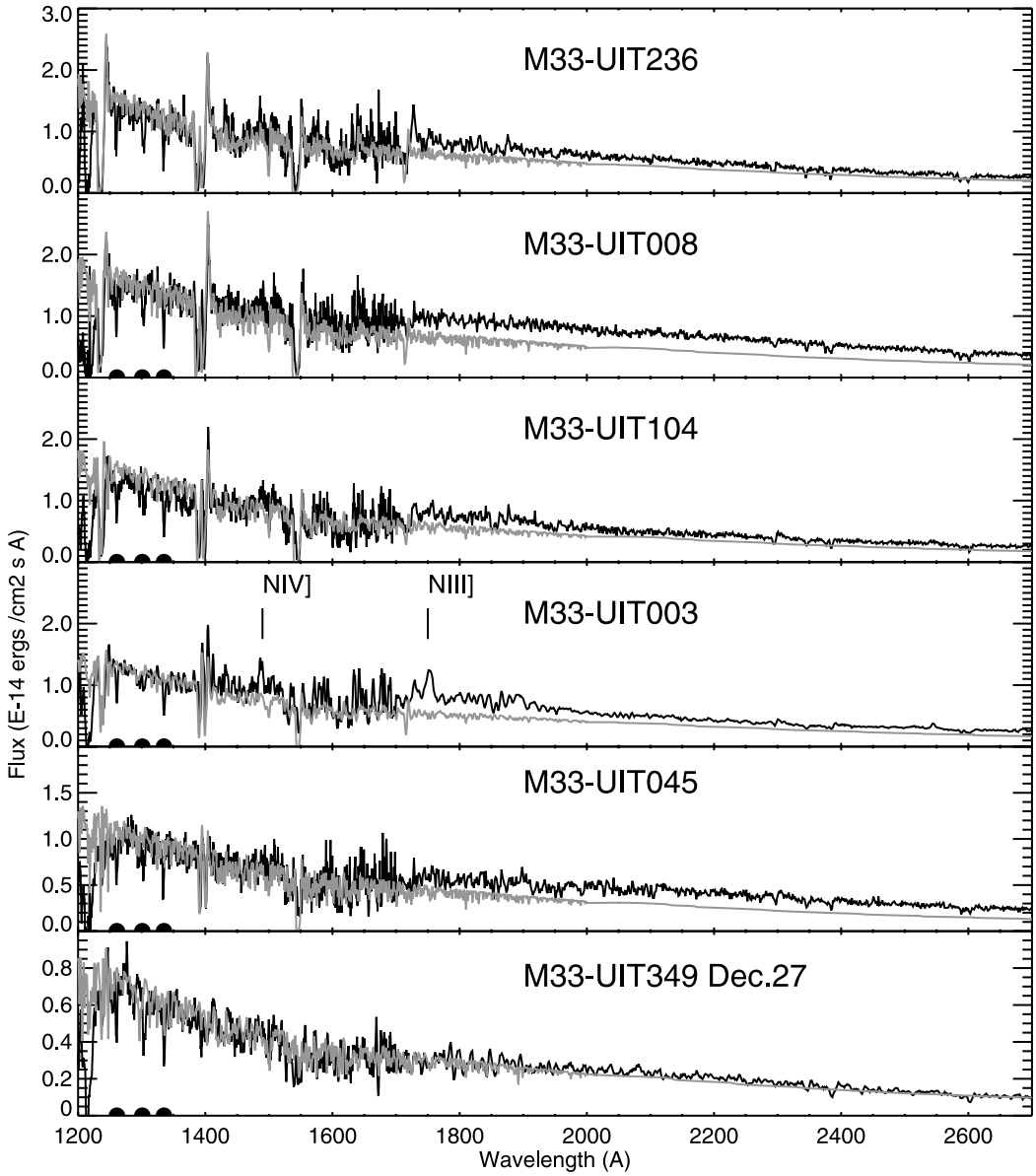

FIG. 7.—Same as in Fig. 6, but the longer wavelength range is shown. The STIS spectra (*solid line*), dereddened for the amount of extinction given in Table 2, and the best-fit models computed with WM-BASIC are shown. A slight flux excess is seen in most spectra beyond ≈1800 Å; its possible origin is discussed in the text. [*See the electronic edition of the Journal for a color version of this figure*.]

Nugis, Crowther, & Willis 1998; Gräefner, Koesterke, & Hamann 2002) and thus higher than what we measure for the Ofpe/WN9 stars. To compare with O-type stars, we use the recent "recipe" (based on theoretical Monte Carlo simulations) from Vink et al. (2000, 2001) for Population I stars and find that the predicted mass-loss rates are of the order of $2 \times 10^{-6}\,M_{\odot}\,\mathrm{yr}^{-1}$ for the first five stars ($[2.4 - 1.7] \times 10^{-6}\,M_{\odot}\,\mathrm{yr}^{-1}$ from M33-UIT236 to M33-UIT045) for solar metallicity and less for metallicity lower than solar (e.g., for $z = 0.1$ times solar, $\dot{M}$ would be lower by a factor of 7). In summary, the values of the mass-loss rates derived for our sample are lower than typical W-R mass-loss rates, but in comparison with predictions from radiation-pressure wind theory for Population I stars, mass loss is enhanced for the hottest stars (M33-UIT236, M33-UIT008, and M33-UIT104), comparable with the predictions for M33-UIT003 and lower than predicted for M33-UIT045 and M33-UIT349. However, as we stressed before, $\dot{M}$ derivations are less reliable for the two latter stars, since the lines are extremely weak. Another result emerging by these comparisons is that mass-loss rate varies within the sample more than we would expect from the variation of the other physical parameters (T_{eff}, L_{bol}, and mass). Because of this and because the UV line strengths do not correlate with optical line strengths observed several years earlier, we suggest that mass-loss rate may vary in time as well. LBV stars also display variable mass-loss rates, which Vink & de Koter (2002) explain in terms of changes in the line driving efficiency. The large spread in mass-loss rates among our sample may also relate to evolutionary effects. The physical conditions of the radiation-pressure–driven wind change during the evolutionary phases from O-type to LBV to W-R, and these classes of objects display very different mass-loss rates and wind velocities, although the stellar luminosity remains basically constant during the transition. According to Lamers & Nugis (2002), the wind changes are mainly due to changes in stellar parameters (radius and gravity) and to a lesser extent to change in surface chemical abundances. The ensemble of our findings consistently points

out that the first four objects in Table 2 are transitioning toward the W-R (WNL) stage through an enhanced mass-loss phase.

All spectra are very well fitted in both continuum flux level and line strength at the short wavelengths (G140L range), while a mismatch between observed flux and model is seen longward for most stars. All stars appear to be pointlike sources at the STIS spatial resolution. The amount of the mismatch (up to 5% at the longer wavelengths) is comparable with the absolute flux confidence level (§ 2.2) and with the uncertainty in the extinction amount and extinction law. A variation in $E(B-V)$ of 0.01 would have an effect comparable with the mismatch seen beyond 1700 Å. However, it would create a larger mismatch at the shorter wavelengths, which are more sensitive to the reddening, and thus was excluded. The amount of extinction $[E(B-V)]$ adopted as our best fit to the spectra is given in Table 2, and the adopted extinction law is a combination of Galactic extinction (foreground) and LMC-type extinction. This was found to be generally the preferable solution, after examining different combinations with all known extinction laws (for other galaxies) concurrently with varying the stellar model parameters. The UV extinction law in M33 is currently being investigated by us with another STIS program, and the results may refine this issue. We attempted to add different blackbody components to the stellar-model fits. While we may visually improve the fit to the observed spectra at the long wavelengths, removing the mismatch, the results would not be significant given that the flux level of a postulated additional component would be up to a few percent that of the luminous hot star. Therefore, we cannot determine at this point whether a faint excess flux, peaking at about 1800 Å or longward, is present in addition to the brighter hot luminous star spectrum, or whether the extinction curve slightly differs from the Milky Way and LMC ones.

Finally, we point out again two remaining possible sources of uncertainty in the present analysis. The first may come from some inconsistency in the WM-BASIC calculations for the cases of extreme parameters such as those of M33-UIT045 and M33-UIT349, where the flux indicates a hot, luminous object but the lack of wind lines (or just of N v in the case of M33-UIT045) indicates an unusually low mass-loss rate. These caveats are discussed at length by Bianchi & Garcia (2002), L. Bianchi, M. Garcia, & J. Herald (2003, in preparation), and M. Garcia & L. Bianchi (2003, in preparation). Second, the amount of shocks in the winds and the effect of the related X-rays on the ionization—which bears on the $T_{\rm eff}$ results—cannot be precisely estimated when only the UV range is available. The *Far-Ultraviolet Explorer* (*FUSE*) range, at shorter wavelengths, contains transitions much more sensitive to this parameter than those in our STIS spectra, primarily the O vi doublet (Bianchi & Garcia 2002; Bianchi et al. 2003). We plan to extend the analysis of the sample to the *FUSE* range as a next step, although the fluxes of these distant objects are at the limit of detection for *FUSE*.

It is interesting to compare our findings with similar objects in other galaxies to verify metallicity effects on the evolution. To our knowledge, no similar modeling of UV spectra has been performed for Ofpe/WN9 stars in the Milky Way or other galaxies. However, previous works, mostly based on optical spectroscopy, provide very useful comparisons. Similarly to our STIS spectra, UV FOS spectra of all the LMC "slash stars" show P Cygni profiles of C iii λ 1176, Si iv $\lambda\lambda$1394, 1403, and N iii $\lambda\lambda$1748, 1752. Other strong lines, C iv $\lambda\lambda$1548, 1550, N v $\lambda\lambda$1238, 1243, He ii λ1640, N iv λ1719, and Al iii $\lambda\lambda$1855, 1863, vary from pure absorption to strong P Cygni profiles in the sample (Pasquali et al. 1997). These authors derive terminal velocities of the order of 400 km s^{-1}, much lower than the wind velocities measured in our sample, and mass-loss rates (from Hα equivalent widths) of $\approx(2-5)\times 10^{-5}\ M_{\odot}\ {\rm yr}^{-1}$, much higher than what we found for the M33 counterparts. The discrepancy may be due to the Hα equivalent width method, where the correction for the underlying photospheric absorption is a very large source of uncertainty (Bianchi & Scuderi 1999). A non-LTE analysis of the optical spectrum of an Ofpe/WN9 star in NGC 300 was performed by Bresolin et al. (2002) using the Hillier & Miller (1998) code. The $T_{\rm eff}$ is lower but the luminosity and the mass-loss rate are higher than the range of values found in our sample. Crowther & Smith 1997 performed a non-LTE analysis of optical spectra of LMC's Ofpe/WN9 stars, which, however, they reclassified as WNL stars (WN9–WN11). They find a range of $T_{\rm eff}$ values that overlaps with the lower end of our range, most of their sample (WN9–WN11) stars having lower values of $T_{\rm eff}$ than ours, and higher $\dot{M}$ values. We caution again that mass-loss rates derived from UV and from optical spectra give often discrepant results (e.g., Crowther, Hillier, & Evans 2002; Bianchi & Garcia 2002) and thus the comparison has to be taken with caution. A more conclusive comparison would require similar analysis of similar data sets.

Support for this work (proposal GO 8207) was provided by NASA through grant GO8207-0197A from the Space Telescope Science Institute, which is operated by the Association of Universities for Research in Astronomy, Inc., under NASA contract NAS5-26555. We are very grateful to Miriam Garcia for computing several WM-BASIC models of the grid used in this work and to Jorick Vink, Lars Koesterke, and Wolf-Rainer Hamann for useful discussions.

REFERENCES

Bianchi, L. 1982a, Proc. Third European *IUE* Conf. (ESA SP-176; Noordwijk: ESA), 251
———. 1982b, Adv. Space Res., 2(9), 293
Bianchi, L., & Garcia, M. 2002, ApJ, 581, 610
———. 2003, The Local Group as an Astrophysical Laboratory, ed. M. Livio (Baltimore: STScI), in press
Bianchi, L., Garcia, M., & Herald, J. 2003, Rev. Mexicana Astron. Astrofis. Ser. Conf., 15, 226
Bianchi, L., & Scuderi, S. 1999, Mem. Soc. Astron. Italiana, 70, 667
Bohannan, B., & Walborn, N. R. 1989, PASP, 101, 520
Bohlin, R. C. 2000, AJ, 120, 437
Bohlin, R. C., Dickinson, M. E., & Calzetti, D. 2001, AJ, 122, 2118
Bohlin R., & Hartig, G. 1998, Instrum. Sci. Rep. (STIS 98-20: Baltimore: STScI)
Bresolin, F., Kudritzki, R. P., Najarro, F., Gieren, W., & Pietrzynski, G. 2002, ApJ, 577, L107
Conti, P. S. 1976, Mem. Soc. R. Sci. Liège, 9, 193
Conti, P. S., & Bohannan, B. 1989, in IAU Colloq. 113, Physics of Luminous Blue Variables, ed. K. Davidson, A. F. Moffat, & H. J. G. L. M. (Dordrecht: Kluwer), 297
Crowther, P. A., Hillier, D. J., Evans, C. J., Fullerton, A. W., De Marco, O., & Willis, A. J. 2002, ApJ, 579, 774
Crowther, P. A., & Smith, L. J. 1997, A&A, 320, 500
Gräfener, G., Koesterke, L., & Hamann, W.-R. 2002, A&A, 387, 244

Hillier, D. J., & Miller, D. L. 1998, ApJ, 496, 407
Krabbe, A., Genzel, R., Drapatz, S., & Rotaciuc, V. 1991, ApJ, 382, L19
Lamers, H. J. G. L. M., Nota, A., Panagia, N., Smith, L. J., & Langer, N. 2001, ApJ, 551, 764
Lamers, H. J. G. L. M., & Nugis, T. 2002, A&A, 395, L1
Langer, N., Heger, A., & Fliegner, J. 1998, in IAU Symp. 189, Fundamental Stellar Properties, ed. T. Bedding, A. J. Booth, & J. Davis (Dordrecht: Kluwer), 343
Maeder, A. 1987, A&A, 173, 247
Maeder, A., & Conti, P. S. 1994, ARA&A, 32, 227
Maeder, A., & Meynet, G. 1994, A&A, 287, 803
Magrini, L., Corradi, R., Mampaso, A., & Perinotto, M. 2000, A&A, 355, 713
Massey, P. 2003, ARA&A, 41, 15
Massey, P., Bianchi, L., Hutchings, J. B., & Stecher, T. 1996, ApJ, 469, 629 (MBHS)
Massey, P., DeGioia-Eastwood, K., & Waterhouse, E. 2001, AJ, 121, 1050
Massey, P., Waterhouse, E., & DeGioia-Eastwood, K. 2000, AJ, 119, 2214
Meynet, G., & Maeder, A. 2000, A&A, 361, 101
———. 2003, A&A, 404, 975
Morris, P. W., Eenens, P. R. J., Hanson, M. M., Conti, P. S., & Blum, R. D. 1996, ApJ, 470, 597
Nieuwenhuijzen, H., & de Jager, C. 1990, A&A, 231, 134
Nota, A., Pasquali, A., Drissen, L., Leitherer, C., Robert, C., Moffat, A., & Schmutz, W. 1996, ApJS, 102, 383
Nota, A., Pasquali, A., Drissen, L., Leitherer, C., Robert, C., & Schmutz, W. 1995, Ap&SS, 224, 261
Nugis, T., Crowther, P., & Willis, A. 1998, A&A, 333, 956
Nugis, T., & Lamers, H. J. G. L. M. 2000, A&A, 360, 227
Pasquali, A., Langer, N., Schmutz, W., Leitherer, C., Nota, A., Hubeny, I., & Moffat, A. 1997, ApJ, 478, 340
Pasquali, A., et al. 1999, A&A, 343, 536
Pauldrach, A. W. A., Hoffmann, T. L., & Lennon, M. 2001, A&A, 375, 161
Stahl, O. 1987, A&A, 182, 229
Stahl, O., Wolf, B., Klare, G., Cassatella, A., Krautter, J., Persi, P., & Ferrari-Toniolo, M. 1983, A&A, 127, 49
Vink, J., & de Koter, A. 2002, A&A, 393, 543
Vink, J. S., de Koter, A., & Lamers, H. J. G. L. M. 2000, A&A, 362, 295
———. 2001, A&A, 369, 574
Walborn, N. 1977, ApJ, 215, 53
———. 1982a, ApJ, 256, 452
———. 1982b, IAU Circ. 3767
Warner, P. J., Wright, M. C. H., & Baldwin, J. E. 1973, MNRAS, 163, 163